Carbon Trends 15 (2024) 100346

Contents lists available at ScienceDirect

Carbon Trends

journal homepage: www.elsevier.com/locate/cartre

Small-angle x-ray scattering analysis of carbon fiber voids considering void length distribution

Daisuke Kimura [a,b], Masahiko Demura [b,c], Kenji Nagata [b,c], Toshihira Irisawa [d], Yoshiki Sugimoto [e], Wataru Takarada [a,*], Masatoshi Shioya [a]

[a] School of Materials and Chemical Technology, Tokyo Institute of Technology, 2-12-1-S8-34 Ookayama, Meguro-ku, Tokyo 152-8552, Japan
[b] Tokyo Tech Academy for Convergence of Materials and Information, Tokyo Institute of Technology, Tokyo, Japan
[c] National Institute for Materials Science (NIMS), Ibaraki, Japan
[d] Department of Chemistry and Biomolecular Science, Faculty of Engineering, Gifu University, Gifu, Japan
[e] Multi-Material Research Institute, National Institute of Advanced Industrial Science and Technology (AIST), Aichi, Japan

ARTICLE INFO

Keywords:
Carbon fibers
Small-angle x-ray scattering
Microvoids

ABSTRACT

The analysis method proposed by Ruland et al. is widely used to analyze the void lengths in carbon fibers, but it could not apply to mesophase pitch-based carbon fibers. We thought that the reason for the inability to analyze pitch-based carbon fibers was the length distribution of voids that Ruland neglected. We investigated an analytical method that considers the length distribution of voids in carbon fibers. The proposed new method could be applied to various carbon fibers from polyacrylonitrile and mesophase pitch. The analysis results revealed that the average length of voids in mesophase pitch-based carbon fibers is not only long but also widely distributed. On the other hand, the voids of carbon fibers tend to be longer as the crystallite length is longer in both polyacrylonitrile-based and mesophase-based carbon fibers. It suggests that the growth of void length is strongly influenced by the growth of crystallites in the plane direction.

1. Introduction

Carbon fibers are light, high-strength materials with outstanding specific strength and elastic modulus. Because of this property, carbon fibers are already widely used in the aerospace industry as an energy-saving material. They are also attracting attention for use as a structural material in other fields, such as the automotive industry. Currently, Most of the commercialized carbon fibers are made from polyacrylonitrile (PAN) [1–5] or mesophase pitch (MPP) [6–10]. PAN-based carbon fibers have relatively high strength, while MPP-based carbon fibers have high elasticity and thermal conductivity because of their high crystallinity. Due to the differences in their properties, they are selectively used in areas that suit their applications. On the other hand, although carbon fibers have high tensile strength, their compressive strength is relatively low [11–16], which limits their applications. This feature is critical when bending deformation is applied, and the fibers buckle and fracture on the compressive deformation side. The compressive strength is mainly affected by the longitudinal length of voids in carbon fibers [15,17]. Thus, analysis of the voids is essential in developing carbon fibers. Since observation of the real image of nano-scale voids is difficult, small-angle x-ray scattering (SAXS) measurements are mainly used. Thünemann and Ruland proposed a method to analyze characteristics of voids such as cross-sectional area, diameter, and length [17].

Sugimoto et al. applied the Ruland method to polyacrylonitrile-based carbon fibers, and a clear relation between the void length and compressive strength was obtained [15]. On the other hand, in MPP-based carbon fiber, void length could not be determined by the Ruland method in most cases. The compressive strength of MPP-based carbon fibers is much lower than that of PAN-based carbon fibers at the same level of tensile modulus [18–20]. Therefore, it is necessary to identify the cause of the low compressive strength of MPP-based carbon fibers to expand the application area of MPP-based carbon fibers.

In this study, an analysis method that extends the Ruland method was developed to be able to be applied to MPP-based carbon fibers. These methods were applied to various carbon fibers, and the characteristics of voids were compared. The scattering intensity of SAXS is caused by the electron density difference between matrix and dispersants. Thus, the method can be applied not only to voids in carbon fibers but also to other structures / objects in materials with uniaxial

* Corresponding author.
E-mail address: takarada.w.aa@m.titech.ac.jp (W. Takarada).

https://doi.org/10.1016/j.cartre.2024.100346
Received 30 November 2023; Received in revised form 15 March 2024; Accepted 17 March 2024
Available online 18 March 2024

symmetry. For example, fibrils or substrate areas in high-strength fibers, component A and B in polymer alloys, and nanofiller-added polymers.

2. Theoretical

The azimuthal intensity $I(s, \phi)$ of small-angle X-ray scattering of carbon fibers at a specific reciprocal space vector magnitude s is expressed as follows [17].

$$s = \frac{2}{\lambda}\sin\theta \tag{1}$$

$$I(s,\phi) = n\rho_m^2 |\Phi_D|^2(s)\cdot\left[|\Phi_L|^2(s\,\phi) *_\phi g_{eq}(\phi)\right] \tag{2}$$

where λ is the X-ray wavelength, θ is the Bragg angle, n is the number of voids, ρ_m is the electron density difference between the void region and the matrix in which the voids are embedded, $\Phi_D(s)$ is the 2D Fourier transform of the shape function of the cross-section, $\Phi_L(s\phi)$ is the 1D Fourier transform of the shape function in the length, $g_{eq}(\phi)$ is the orientation distribution function of the long axes of the voids, and $*_\phi$ stands for convolution in ϕ [17].

If s is fixed in Eq. (2), it can be transformed as a function of ϕ as follows.

$$I_s(\phi) = C_s\cdot\left[|\Phi_L|^2(s\,\phi) *_\phi g_{eq}(\phi)\right] \tag{3}$$

If $|\Phi_L|^2(s\phi)$ and $g_{eq}(\phi)$ follow Gaussian functions, respectively, the relation in Eq. (4) holds.

$$\left(\Delta\phi_{fiber}\right)^2 = \left(\Delta\phi_L\right)^2 + \left(\Delta\phi_g\right)^2 \tag{4}$$

where $\Delta\phi_{fiber}$ is the full width at half maximum when fitting $I_s(\phi)$ with a Gaussian function, and $\Delta\phi_L$ and $\Delta\phi_g$ are the full width at half maximum of $|\Phi_L|^2(s\phi)$ and $g_{eq}(\phi)$, assuming they follow Gaussian functions. Also, $|\Phi_L|^2(s\phi)$ and $g_{eq}(\phi)$ are expressed as in Eqs. (5) and (6).

$$|\Phi_L|^2(s\,\phi_L) = c_{void}\exp\left[-\pi {L_3}^2 s^2 {\phi_L}^2\right] \tag{5}$$

$$g_{eq}(\phi_g) = c_{orient}\exp\left[-\frac{4\ln 2}{\left(\Delta\phi_g\right)^2}{\phi_g}^2\right] \tag{6}$$

where c_{void} and $c_{orinent}$ are constants and L_3 is the longitudinal length of the void.

From the relations in Eqs. (4), (5), and (6), the model proposed by Ruland et al. approximates the azimuthal scattering intensity at a certain scattering angle 2θ in a single void as a Gaussian function and assumes that the orientation distribution function at the tilt from the fiber axis when the void is projected onto the detector is a Gaussian function, so the following equation holds [15,17].

$$B^2\cdot s^2 = \frac{1}{{L_3}^2} + {B_o}^2\cdot s^2 \tag{7}$$

L_3 is the longitudinal length of the void, and B is the integral width when fitting the azimuthal scattering intensity with a Gaussian function. From Eq. (7), by measuring the integral width B of the scattering intensity in each azimuthal direction at various scattering angles, a plot of (B^2s^2) vs. s^2 can be obtained, and the void length L_3 can be derived from the square of the intercept. The advantage of the Ruland method is that information on various scattering angles is included to obtain L_3, making it an accurate and reproducible analysis method. On the other hand, there are some cases described later, in which the intercept became a negative value, and it was impossible to calculate the length of the voids, even when fitting in any s^2 region. This is especially a problem that frequently occurs with MPP-based carbon fibers.

The Ruland method was considered to be the constant void length. We modified the Ruland model under two assumptions. The first assumption is that the void shape is not constant and follows a distribution function, P(t). The distribution function is defined as the ratio of the product of the number and volume squared of the void of a certain shape. The other assumption is that the orientation depends on the void length, longer voids have higher orientation. The equations for the model with these assumptions were derived as follows.

First, when the void length exists only at t, the azimuthal profile of the scattering intensity at the scattering angle s_o is given by Eq. (8).

$$\begin{aligned} I(s_o,\phi,t) &= C(t)\cdot\left[|\Phi_L|^2(s_o\phi,t) *_\phi g_{eq}(\phi)\right] \\ &= c_{void}\; c_{orient}\; C(t) exp\left[-\frac{4\ln 2}{\left(\Delta\phi_{L,t}\right)^2 + \left(\Delta\phi_g\right)^2}\phi^2\right] \\ &= D(t) exp\left[-\frac{4\ln 2}{\frac{4\ln 2}{\pi t^2 {s_o}^2} + \left(f(t)\right)^2}\phi^2\right] \\ &= D(t)\cdot I_o(s_o,\phi,t) \end{aligned} \tag{8}$$

where C and D (= $c_{void}\; c_{orinent}\; C$) are variables with respect to t and constants with respect to ϕ. $\Delta\phi_{L,t}$ is full width at half maximum of $|\Phi_L|^2(s\phi,\, t)$, which is $|\Phi_L|^2(s\phi)$ when the void length L_3 is t. f(t) is obtained from the second assumption, a dependence function of void length and orientation. From the first assumption, the true scattering intensity in this model is derived as follows

$$\begin{aligned} I_{true}(s_o,\phi) &= \int I_o(s_o,\phi,t)\cdot P(t-t_o)dt \\ &= I_o(s_o,\phi,t_o) *_{t_o} P(t_o) \end{aligned} \tag{9}$$

$$P(t) = D(t)/D_o \tag{10}$$

Assuming that P(t) follows a Gaussian distribution with respect to t, where t_o is the peak center (the average of the void lengths), Eqs. (11) and (12) are derived when $f(t) = \sqrt{\beta}\pi\ /\ t$. The validity of $f(t)$ in such a function of t is demonstrated in Supplementary.

$$I_{fiber}(s\,\phi) = c_{fiber}\exp\left(-\frac{4\ln 2\cdot {t_o}^2}{\alpha + (\Delta t)^2\phi^2}\phi^2\right) \tag{11}$$

$$\alpha = \frac{4\ln 2}{\pi s^2} + \beta\pi^2 \tag{12}$$

$I_{fiber}(s\phi_{fiber})$ is the scattering intensity at a certain scattering angle in the SAXS image of a carbon fiber, ϕ is the scattering angle from the equatorial direction on the SAXS images, t_o is the mean length of voids in the longitudinal direction, Δt is the full width at half maximum of P(t), c_{fiber} and β are coefficients.

In this paper, the mean and distribution width of the void length in carbon fibers are analyzed by using Eqs. (11) and (12). It should be noted that, unlike the Ruland method, this analysis method uses only the scattering intensity at a certain s. When using this method, it is necessary to analyze the data at various scattering angles and to look at the average value of the data to see if there are any other factors, such as

Table 1
Thickness L_c, length L_a, orientation f_c, interlayer spacing d_{002}, and (10) reflection plane spacing d_{10} of the crystallites were identified by WAXD measurements.

	L_c [nm]	d_{002} [nm]	f_c []	L_a [nm]	d_{10} [nm]
PAN-1	1.73	0.343	0.78	2.670	0.650
PAN-2	4.77	0.338	0.91	8.98	0.659
PAN-3	5.88	0.338	0.93	10.7	0.659
MPP-1	6.76	0.338	0.91	7.25	0.658
MPP-2	8.94	0.335	0.96	13.1	0.658
MPP-3	10.4	0.339	0.95	14.3	0.658
MPP-4	7.46	0.337	0.91	7.59	0.659
MPP-5	9.30	0.339	0.94	9.33	0.660
MPP-6	10.2	0.337	0.95	12.3	0.662

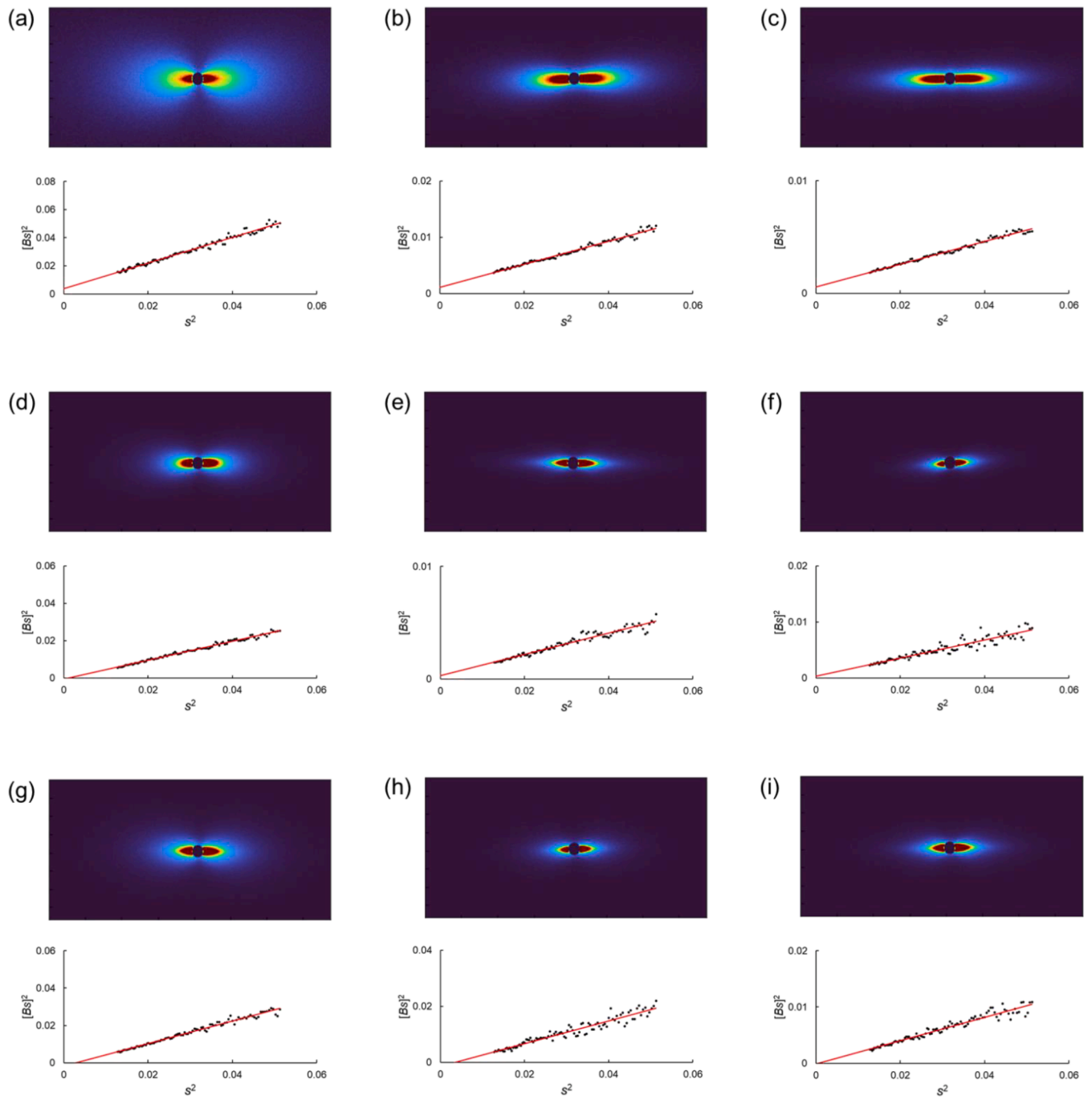

Fig. 1. 2D SAXS images of carbon fibers and the plots used in the Ruland method. The red line in the graph is the result of linear regression. ((a) PAN-1, (b) PAN-2, (c) PAN-3, (d) MPP-1, (e) MPP-2, (f) MPP-3, (g) MPP-4, (h) MPP-5, and (i) MPP-6).

parasitic scattering, that could disturb the data.

3. Experiment

3.1. Materials

Six MPP-based carbon fibers and three PAN-based carbon fibers were used for comparison. The thickness, length, and orientation of the crystallites were identified by wide-angle X-ray diffraction (WAXD) measurements [21,22]. These values are summarized in Table 1.

The specimens of SAXS measurement were prepared from a bundle of carbon fibers. In preparing the specimens, the sizing material on carbon fibers was removed by ultrasonic treatment with acetone.

3.2. Methods

The X-ray source for WAXD and SAXS measurements was Cu K-α (wavelength: 0.1542 nm).

In Table 1, the thickness of the crystallites L_c was derived from the peak position and the half-width at half maximum in the low angle side of (002) by the method proposed by Shioya and Takaku. [21,22]. f_c was derived from the full width at half maximum in the azimuthal direction at the peak position of (002). The length of carbon crystallites along the fiber axis L_a was measured using the peak position and half-width at low angle side of (10) in the fiber axial direction with tilting the fiber at an angle of θ [degree] (21°) to the incident X-ray beam [21,22].

In the SAXS analysis, s^2-B^2s^2 plots were conducted using the fitting

Table 2
Results analyzed by the Ruland method. L_3 is the longitudinal length of the void, and f_v is the orientation degree of the void.

	L_3 [nm]	f_v
PAN-1	16.34	0.71
PAN-2	29.69	0.86
PAN-3	41.74	0.91
MPP-1	–	0.79
MPP-2	58.52	0.91
MPP-3	51.46	0.88
MPP-4	–	0.77
MPP-5	–	0.81
MPP-6	–	0.86

method with Gaussian functions in the method proposed by Ruland et al. Next, a comparison was conducted between the fitting results at each scattering angle using the new analysis method (Eqs. (11) and (12)) and the fitting results in the Gaussian function used in the Ruland method. Finally, the values obtained by the new analysis method for each carbon fiber were compared.

4. Result and discussion

4.1. Ruland method

The SAXS images of carbon fibers are shown in Fig. 1. The s^2-B^2s^2 plots are shown to the right of the SAXS images.

The longitudinal length of the voids L_3 and the orientation of the voids f_v obtained by Ruland method were as shown in Table 2. The orientation of the voids was calculated from the slope in Fig. 1 [15]. The length of the voids L_3 was calculated from the intercept in Fig. 1. An analytical result for L_3 could not be obtained in some carbon fibers because its intercept was negative.

4.2. Method considering length distribution of voids

According to the Ruland method, the azimuthal profile of scattering intensity is Gaussian. Fig. 2 shows the azimuthal profiles at a scattering angle of 2θ (CuKα) = 1.0 [degrees] (s = 0.113 [nm^{-1}]) as an example. The blue line is the value fitted by the Gaussian function. It was clarified that many carbon fibers, especially mesophase MPP-based carbon fibers, could not be analyzed properly using Gaussian function.

Fig. 2 shows that some peaks are close to Gaussian function while others are more Lorentzian function. The difference in the tail of these peaks is related to the void length distribution proposed in this paper. Fig. 3 shows the characteristics of the function (Eq. (11)) when the mean void length t and the full width at half maximum of the void length distribution Δt are varied for s = 0.2 [nm^{-1}]. In this paper, $\beta = (5.03)^2$ was used for Eq. (11). This value β is based on the relation between the void length and orientation of carbon fibers obtained from Ruland method. The details are described in the Supplementary Information. It is necessary to determine appropriate β value when applying Eq. (11) to other materials (e.g., organic polymer fibers and nanofiller-added materials).

Fig. 3(a) compares the peaks when Δt is varied and t_o is fixed. When the void length distribution is wider, the tail of the peak is larger. Fig. 3 (b) compares the peaks when Δt is fixed and t_o is varied. The peak becomes sharper when the mean value of the void length increases. Fig. 4 shows the results of fitting the azimuthal profiles of each carbon fiber by using Eq. (11) with the abovementioned characteristics. The results show that good fitting was obtained for all the carbon fibers.

The analysis described above resulted in the mean and full width at half maximum of the void length at specific scattering angle s. Fig. 5 shows the analysis results at the scattering angle range of 1–2.5 [degree], which is the range where the signal is not significantly affected by noise and is not affected by total reflection, which is a parasitic scattering. The values changed with the scattering angle in some carbon fibers, but variation was not so large. Thus, average value among scattering angle 1 – 2.5 [degree] was used as the representative values for

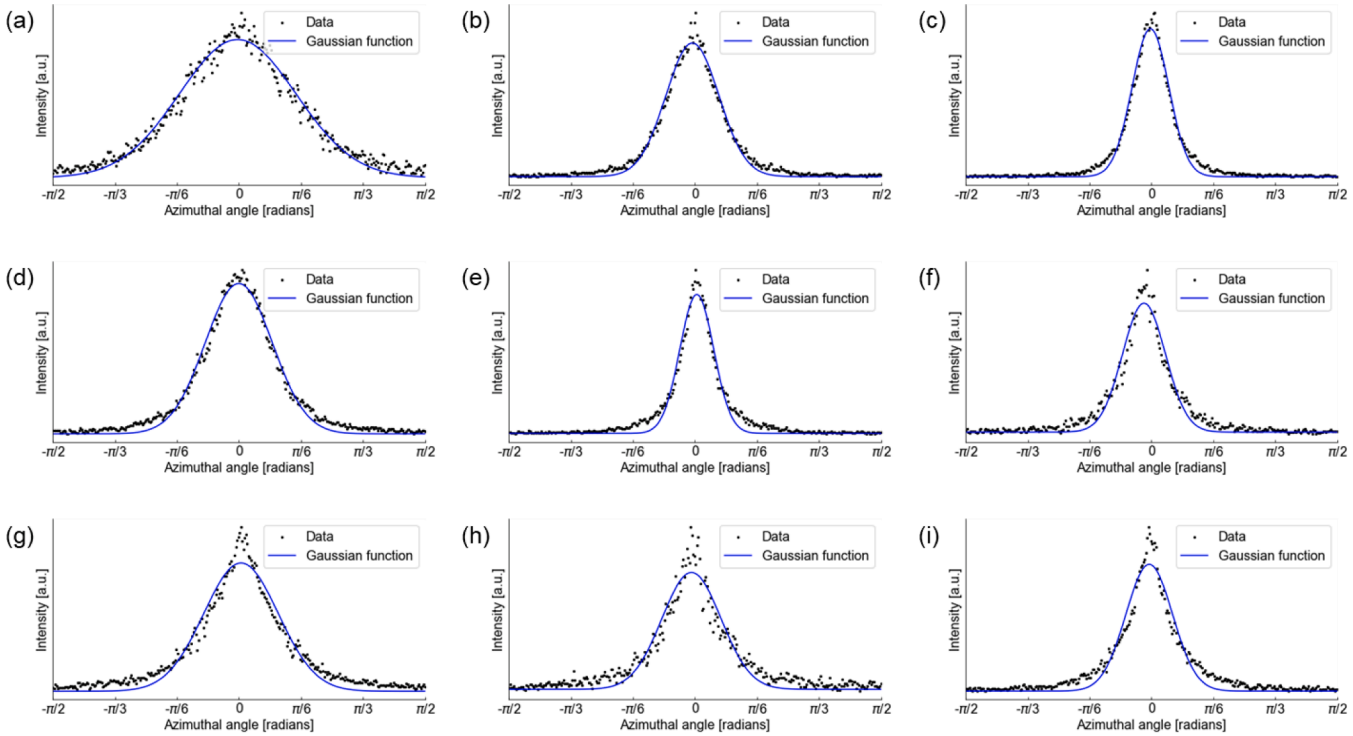

Fig. 2. Scattering profiles in the azimuthal direction in SAXS. The blue line is the result of fitting with a Gaussian function. ((a)PAN-1, (b)PAN-2, (c)PAN-3, (d)MPP-1, (e)MPP-2, (f)MPP-3, (g)MPP-4, (h)MPP-5, and (i)MPP-6).

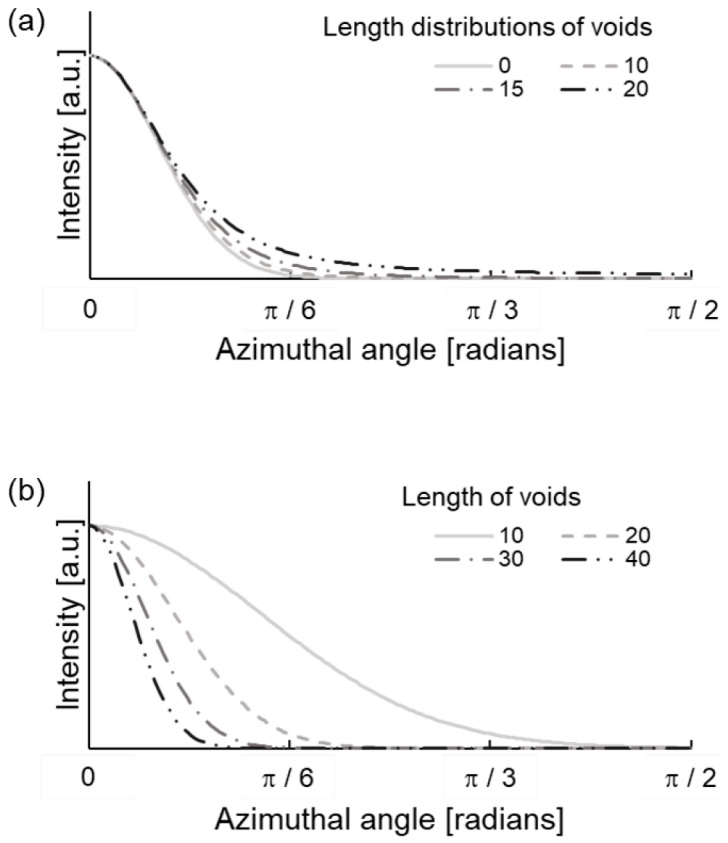

Fig. 3. Features of the analytical function (Eq. (11)) derived in this study. Peaks (a) for different length distributions of voids and (b) for different average lengths of voids.

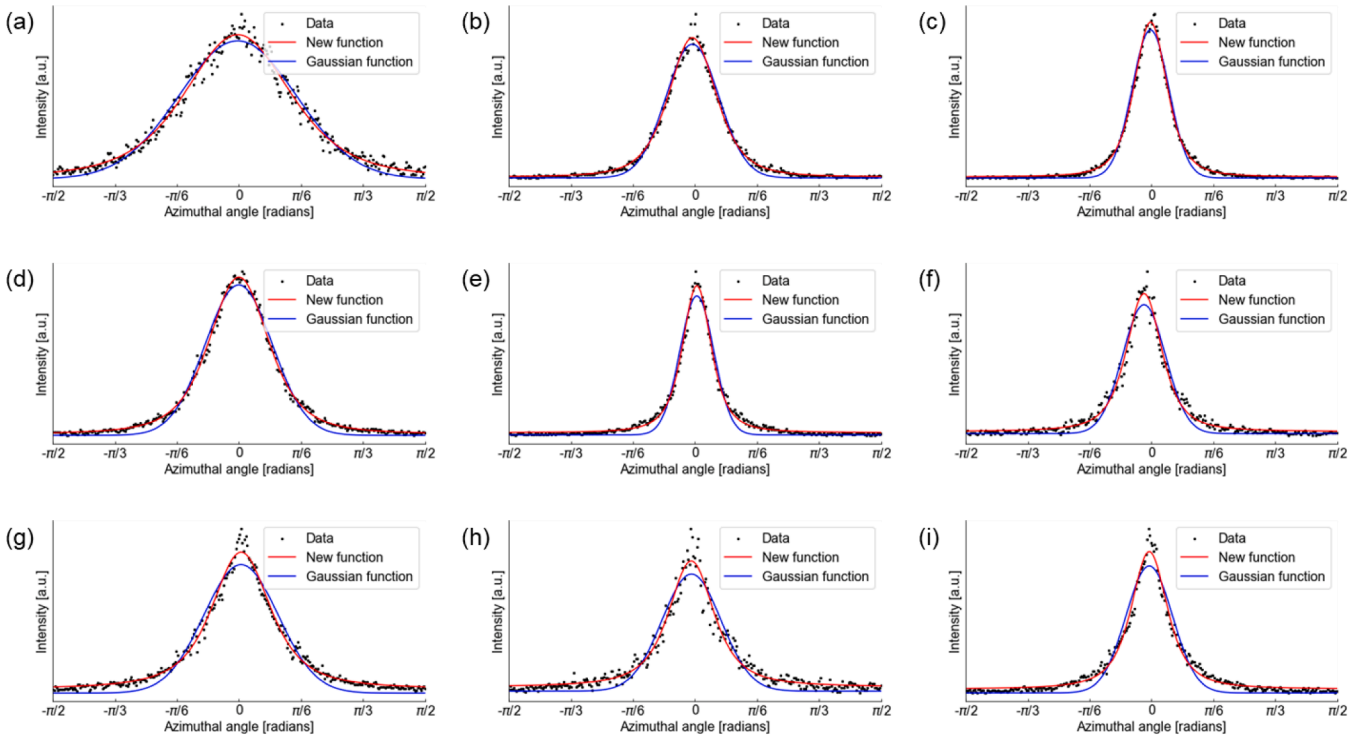

Fig. 4. Results of fitting the data in Fig. 2 with an analytical function. The red line is the result of fitting with the new function (Eq. (11)), and the blue line is the result of fitting with the Gaussian function. ((a)PAN-1, (b)PAN-2, (c)PAN-3, (d)MPP-1, (e)MPP-2, (f)MPP-3, (g)MPP-4, (h)MPP-5, and (i)MPP-6).

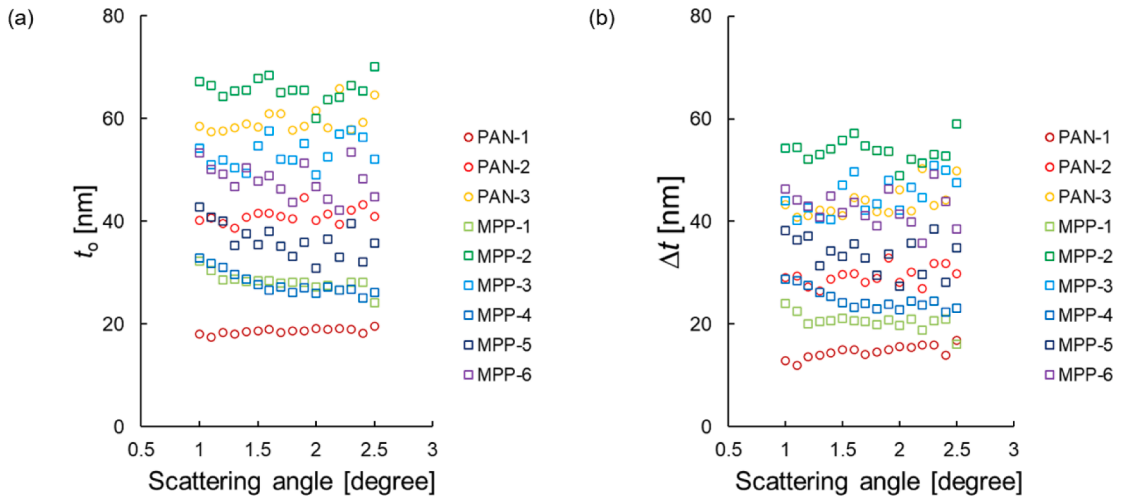

Fig. 5. (a) Mean and (b) full width at half-maximum of the distribution P(t) in the longitudinal length of the voids.

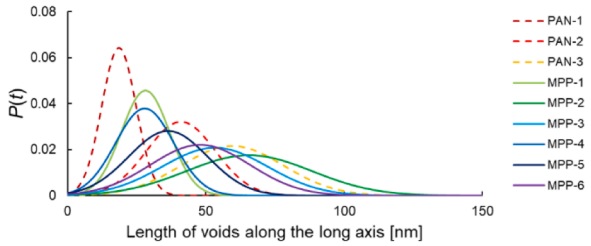

Fig. 6. Distribution function of voids in carbon fibers.

each carbon fiber in this study. Fig. 6 shows the distribution P related to the void lengths inside carbon fibers using the average of the respective values in Fig. 5.

As shown in Fig. 6, the longer the average length of voids, the wider the void length distribution. Also, carbon fibers with larger crystallite lengths showed a tendency for the average length of voids to be larger. Furthermore, it was found that there are small voids as well as large voids in carbon fibers with large crystallite size such as MPP-2, 3, 5, and 6. This result suggests that not all of the voids are growing larger, but some of them are growing, or small voids are growing slightly and connecting with other voids when crystallizing during the higher-temperature sintering process. MPP based carbon fiber has slightly broader distribution of void lengths than PAN carbon fiber which has similar mean void length. This is particularly obvious when comparing PAN-2 and MPP-5, which have similar mean values of void lengths. It can be seen that MPP-5 has a slightly smaller mean value than PAN-2. However, both have voids nearly 75 nm in length due to the larger distribution width of MPP-5 than PAN-2.

Fig. 7 shows the relationship between crystallite size and void length. Error bars are the full width at half maximum of P(t). As shown in Fig. 7 (b), the voids are longer when the crystallite lengths are longer in both of PAN and MPP based carbon fibers. On the other hand, the relationship between crystallite thickness and void length tends to differ depending on the precursor. It suggests that the growth of void length is strongly influenced by the growth of crystallites in the plane direction.

5. Conclusion

We proposed a new analysis method to analyze various carbon fibers, including MPP-based carbon fibers, by extending the Ruland method. The new analytical method revealed the following.

1. The azimuthal profile can be represented better by considering the length distribution of the voids.
2. In carbon fibers, the longer the average length of voids, the wider the void length distribution.
3. MPP-based carbon fibers have voids with wider length distribution.

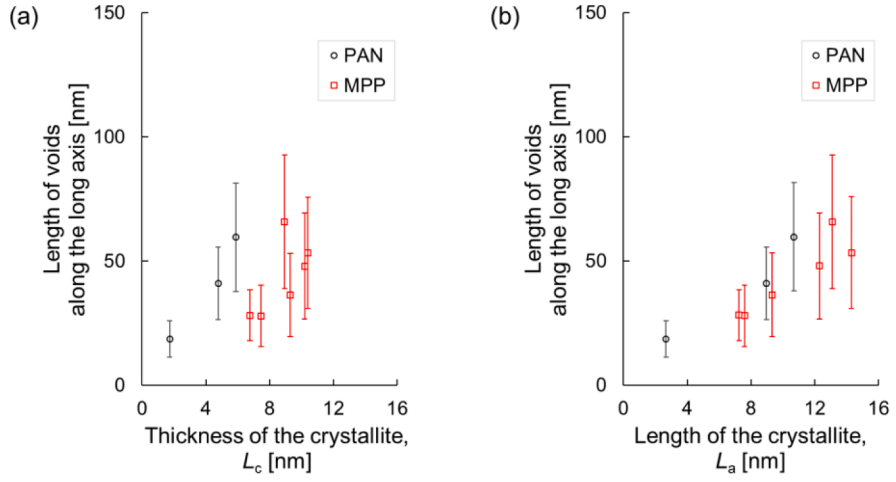

Fig. 7. Relationship between the crystallite size ((a) the thickness and (b) the length) and length of voids along the long axis.

4. Regardless of the precursor, the voids of carbon fibers tend to be longer as the crystallite length is longer.

CRediT authorship contribution statement

Daisuke Kimura: Writing – original draft, Visualization, Methodology, Formal analysis, Data curation, Conceptualization. **Masahiko Demura:** Supervision, Methodology, Formal analysis. **Kenji Nagata:** Supervision, Formal analysis. **Toshihira Irisawa:** Methodology, Formal analysis, Conceptualization. **Yoshiki Sugimoto:** Methodology, Formal analysis, Conceptualization. **Wataru Takarada:** Writing – review & editing, Visualization, Validation, Methodology, Formal analysis, Conceptualization. **Masatoshi Shioya:** Supervision, Conceptualization.

Declaration of competing interest

The authors declare that they have no known competing financial interests or personal relationships that could have appeared to influence the work reported in this paper.

Data availability

Data will be made available on request.

Supplementary materials

Supplementary material associated with this article can be found, in the online version, at doi:10.1016/j.cartre.2024.100346.

References

[1] W. Watt, W. Johnson, Mechanism of oxidisation of polyacrylonitrile fibres, Nature 257 (1975) 210–212, https://doi.org/10.1038/257210a0.
[2] E. Fitzer, Pan-based carbon fibers—present state and trend of the technology from the viewpoint of possibilities and limits to influence and to control the fiber properties by the process parameters, Carbon 27 (5) (1989) 621–645, https://doi.org/10.1016/0008-6223(89)90197-8.
[3] H. Okuda, R.J. young, D. Wolverson, F. Tanaka, G. Yamamoto, T. Okabe, Investigating nanostructures in carbon fibres using Raman spectroscopy, Carbon 130 (2018) 178–184, https://doi.org/10.1016/j.carbon.2017.12.108.
[4] D. Jang, M.E. Lee, J. Choi, S.Y. Cho, S. Lee, Strategies for the production of PAN-Based carbon fibers with high tensile strength, Carbon 186 (2022) 644–677, https://doi.org/10.1016/j.carbon.2021.10.061.
[5] H. Zhou, J. Zhu, H. Wang, Tuning of structural/functional feature of carbon fibers: New insights into the stabilization of polyacrylonitrile, Polymer (Guildf) 282 (2023) 126157, https://doi.org/10.1016/j.polymer.2023.126157.
[6] S. Otani, On the carbon fiber from the molten pyrolysis products, Carbon 3 (1) (1965) 31–34, https://doi.org/10.1016/0008-6223(65)90024-2.
[7] I. Mochida, S.H. Yoon, N. Takano, F. Fortin, Y. Korai, K. Yokogawa, Microstructure of mesophase pitch-based carbon fiber and its control, Carbon 34 (8) (1996) 941–956, https://doi.org/10.1016/j.carbon.2014.07.068.
[8] F.G. Emmerich, Young's modulus, thermal conductivity, electrical resistivity and coefficient of thermal expansion of mesophase pitch-based carbon fibers, Carbon 79 (2014) 274–293, https://doi.org/10.1016/j.carbon.2022.08.033.
[9] J. Choi, Y. Lee, Y. Chae, S. Kim, T. Kim, S. Lee, Unveiling the transformation of liquid crystalline domains into carbon crystallites during carbonization of mesophase pitch-derived fibers, Carbon 199 (2022) 288–299, https://doi.org/10.1016/j.carbon.2022.02.062.
[10] H. Shimanoe, T. Mashio, H. Nakashima, S. Ko, Y. Jeon, K. Nakabayashi, J. Miyawaki, S. Yoon, Correlation between molecular stacking and anisotropic texture in spinnable mesophase pitch, Carbon 192 (15) (2022) 395–404, https://doi.org/10.1016/j.carbon.2023.118510.
[11] T. Ohsawa, M. Miwa, M. Kawade, E. Tsushima, Axial compressive strength of carbon fiber, J. Appl. Polym. Sci. 39 (8) (1990) 1733–1743, https://doi.org/10.1002/app.1990.070390811.
[12] M. Nakatani, M. Shioya, J. Yamashita, Axial compressive fracture of carbon fibers, Carbon 37 (1999) 601–608, https://doi.org/10.1016/S0008-6223(98)00230-9.
[13] N. Oya, D.J. Johnson, Longitudinal compressive behaviour and microstructure of PAN-based carbon fibres, Carbon 39 (5) (2001) 635–645, https://doi.org/10.1016/S0008-6223(00)00147-0.
[14] D. Loidl, O. Paris, M. Burghammer, C. Riekel, H. Peterlik, Direct Observation of Nanocrystallite Buckling in Carbon Fibers under Bending Load, Phys. Rev. Lett. 95 (2005) 225501, https://doi.org/10.1103/PhysRevLett.95.225501.
[15] Yoshiki Sugimoto, Masatoshi Shioya, Katsuhiro Yamamoto, Shinichi Sakurai, Relationship between axial compression strength and longitudinal microvoid size for PAN-based carbon fibers, Carbon 50 (8) (2012) 2860–2869, https://doi.org/10.1016/j.carbon.2012.02.053.
[16] K. Lu, W. Zhu, Q. Su, G. Li, X. Yang, Correlation between compression strength and failure mechanism of carbon fiber composite with tailored modulus of amide acid/SiO2 synergistically stiffened epoxy matrix, Compos. Sci. Technol. 202 (20) (2021) 108593, https://doi.org/10.1016/j.compscitech.2020.108593.
[17] A.F. Thünemann, W. Ruland, Microvoids in Polyacrylonitrile Fibers: A Small-Angle X-ray Scattering Study, Macromolecules 33 (5) (2000) 1848–1852, https://doi.org/10.1021/ma991427x.
[18] S. Kawabata, Measurement of the Transverse Mechanical Properties of High-performance Fibres, J. Textile Inst. 81 (4) (1990) 432–447, https://doi.org/10.1080/00405009008658721.
[19] G.J. Hayes, D.D. Edie, J.M. Kennedy, The recoil compressive strength of pitch-based carbon fibres, J. Mater. Sci 28 (1993) 3247–3257, https://doi.org/10.1007/BF00354243.
[20] A.H. Shinohara, T. Sato, F. Saito, T. Tomioka, Y. Arai, A novel method for measuring direct compressive properties of carbon fibres using a micro-mechanical compression tester, J. Mater. Sci 28 (1993) 6611–6616, https://doi.org/10.1007/BF00356404.
[21] M. Shioya, A. Takaku, Wide-angle X-ray diffraction of materials comprising layer-type molecules, Acta. Cryst. A44 (1988) 150–157, https://doi.org/10.1107/S0108767387009796.
[22] M. Shioya, A. Takaku, Characterization of crystallites in carbon fibres by wide-angle X-ray diffraction, J. Appl. Crystallogr 22 (3) (1989) 222–230, https://doi.org/10.1107/S0021889888014256.